Sub-second Dynamic X-ray Micro-CT and Fast Phase-sensitive Multi-contrast Micro-CT with a Laboratory Source

Harry Allan[ab*], Oriol Roche i Morgó[ab], Carlos Navarrete-Leon[ab], Yunpeng Jia[ab], and Marco Endrizzi[ab]

[a]Department of Medical Physics and Biomedical Engineering, University College London, London, UK
[b]X-ray Microscopy and Tomography Laboratory, The Francis Crick Institute, London, UK

ABSTRACT

A rotating-anode x-ray source and custom-built sCMOS-based detector have been integrated into a lab-based micro-CT system to demonstrate full CT acquisition in as little as 132 ms. This has been used to examine the expansion of a polymer foam in 4D, with a temporal resolution of 2 Hz. The system is easily adapted to carry out fast phase-sensitive multi-contrast CT with sub-10 s CT acquisition times. This is made possible through the beam-tracking technique, which is capable of multi-contrast CT using only a single shot per projection angle, while also being compatible with incoherent sources. This paves the way to dynamic, phase-sensitive, multi-contrast micro-CT in the laboratory.

Keywords: X-ray tomography, dynamic imaging, tomoscopy, 4D imaging, x-ray phase-contrast

1. INTRODUCTION

X-ray micro computed-tomography (micro-CT) is a non-destructive technique providing precise volumetric representations of samples, lending it to use in a large range of fields including medical sciences, materials engineering, and metrology.[1] Its non-destructive nature allows repeated longitudinal testing of the same sample, which when carried out quickly, makes it particularly useful for in-situ and dynamic experiments with materials and processes that change over time. Such experiments have been carried out across a number of topics including food science,[2,3] additive manufacturing,[4,5] and biomedical sciences.[6–8] A common theme amongst these applications is that most leverage the high brilliance and absolute flux available at synchrotron sources to allow the short detector exposures required for such fast imaging. Combining this flux with custom detectors and end stations has allowed ultra-fast synchrotron tomography with full volume acquisition times down to few-to-tens of ms.[9–11] In addition, the coherence and brilliance of synchrotron facilities make phase-contrast techniques, those that derive contrast from phase changes in the wavefront, a routine imaging activity. Phase contrast techniques enable imaging of low-attenuating materials,[12] and allow significant dose reductions for sensitive samples,[13] making them also an important tool in dynamic imaging.

Thanks to developments in efficient detectors and laboratory x-ray tube sources, fast and dynamic experiments have also become a reality outside of large-scale facilities.[14] Numerous examples exist of experiments on the scale of 8-12 s per CT,[15–17] down to cutting-edge speeds of 0.5 s per CT.[18] These experiments have used a variety of custom and commercial systems, where the choice of system components and acquisition parameters are vital for collecting sufficient data and statistics for image reconstruction. We refer readers to an excellent review on fast lab-based CT for an overview of the considerations for such systems.[14]

A number of techniques have also been developed to allow phase-contrast x-ray imaging with lower-coherence laboratory sources, including but not limited to free-space propagation,[19] grating interferometry (GI),[20] edge-illumination,[21] and beam-tracking.[22] Some techniques are also sensitive to the dark-field signal, which indicates the presence of sub-pixel microstructures.[23,24] Alongside dose reduction for potential in-vivo studies,[25]

*harry.allan.21@ucl.ac.uk

Developments in X-Ray Tomography XV, edited by Bert Müller, Ge Wang,
Proc. of SPIE Vol. 13152, 131520O · © 2024 SPIE
0277-786X · doi: 10.1117/12.3028059

these additional contrast channels provide opportunities to measure sample changes in dynamic studies that are not visible through standard attenuation imaging.[26,27] Of particular interest to this work is the recent demonstration of dynamic dark-field tomography with a laboratory GI system, as a potential tool to monitor cryoablation procedures.[28]

We demonstrate a custom built laboratory x-ray micro-CT system, capable of being adapted to a range of experiments but with an emphasis on sub-second tomography acquisition speeds. The system enables both fast individual scans and also the possibility to probe sample dynamics on the sub-second timescale. We also briefly demonstrate a simple modification to the system that allows its fast capabilities to be leveraged for fast and dynamic phase-sensitive imaging. We utilise beam-tracking,[22] which falls into a broader class of techniques which apply amplitude modulation to the x-ray beam[29–33] to make possible simultaneous retrieval of attenuation, phase, and dark-field projections from a single shot. This single shot nature in particular makes beam-tracking suitable for fast imaging, without the overheads associated with other methods that require multiple shots and optical element movements.

2. METHODS

A custom system has been developed with components tailored towards the demands of fast and dynamic imaging experiments. X-rays are generated using a 1.2 kW rotating anode x-ray source (Rigaku MicroMax 007-HF, Mo anode), enabling a high x-ray flux at a moderate focal spot size. An air bearing rotation stage (ESS Mikromeckanik GmbH) was employed to enable fast and accurate rotation of the sample for tomography. The system used a custom-built detector, based upon a sCMOS camera (Hamamatsu Orca-Flash4.0 v3) coupled via visible-light optics to a high light-yield scintillator screen (Lanex Regular), resulting in an effective pixel size of 28.5 μm. The choice of a lens-based system for the detector enables versatility, with both optics and scintillator easily swapped in response to changing demands on detection efficiency and spatial resolution.

For the fast micro-CT system, the total system length was set to 39 cm with a geometrical magnification of 1.36. This geometry was chosen according to the source divergence, that limited the field-of-view (FOV) to 8.3 x 8.3 mm^2, at this distance. The detector was operated in 2x2 binning mode (allowing faster detector readout, a reduction in Nyquist sampling requirements, and a 4x increase in photon statistics[14]) resulting in sample plane voxel dimensions of 42 x 42 x 42 μm^3. The source was operated at 40 kV 30 mA.

A simple high-contrast phantom, consisting of several 400 μm borosilicate spheres glued to a plastic straw, was used to assess attainable scanning speeds and the interplay with contrast-to-noise ratio (CNR). Progressively faster scans were carried out, making use of sCMOS sub-array readout to increase the maximum frame rate to the order of 1000 fps, at the cost of vertical FOV. Volumes were subsequently reconstructed using the Feldkamp-Davis-Kress (FDK) algorithm[34] implemented in the Astra toolbox.[35] The acquisition parameters for these tests are summarised in table 1.

$\mathbf{T_{CT}}$ [ms]	$\mathbf{N_{proj}}$	$\mathbf{T_{exp}}$ [ms]	Reconstruction volume [voxels]
696	348	2	200 x 200 x 200
418	348	1.2	200 x 200 x 128
132	131	1	200 x 200 x 104

Table 1: Acquisition parameters for the series of static fast tomography tests. Parameters describe the time for one full CT acquisition T_{CT}, the number of projections N_{proj}, the exposure time per projection T_{exp}, and the size of the reconstructed volume (after 2x2 binning). Reaching higher frame rates required that only a subset of the detector rows were read out, reducing the vertical FOV.

Next, the dynamic capabilities of the system were demonstrated through the 4D imaging of an expanding polymer foam, with a scan time of $T_{CT} = 510$ ms. The scan time was chosen to allow the use of the entire illuminated FOV without requiring sub-array readout, while being fast enough to limit motion blur due to sample movement. Data was continuously acquired for a period of 2 minutes with an exposure time of 2.5 ms, resulting in a total of 48,000 projections. Acquiring 15.2 GB of data over the course of 2 minutes required that data was streamed directly to the PC RAM and later written to the hard drive once the acquisition had finished. After

a pre-processing step with an FFT-based ring removal algorithm from the Algotom toolbox,[36] volumes were reconstructed from each set of 204 projections (180° + cone angle), using both the FDK algorithm and by an Astra implementation of the simultaneous iterative reconstruction technique (SIRT), using 40 iterations and a non-negativity constraint. To initiate the experiment, the foam was simply compressed by hand and allowed to freely expand.

Finally, the system was adapted to make possible fast multi-contrast phase-sensitive micro-CT. The inclusion of a periodic 1D attenuation mask, with aperture of 17 μm and period of 98 μm, structured the beam into a pattern of beamlets. By using a moments-based approach to analyse the sample-induced perturbations of these beamlets, it is possible to extract the attenuation, differential phase, and dark-field signals from only a single shot per projection angle.[18,22] The scintillator was swapped to a Scintacor Ultrafine+, featuring a smaller point spread function (PSF), to improve the visibility of the periodic pattern. In the initially non-optimised system demonstrated, the source-to-mask distance was set to 79 cm, mask-to-sample 5 cm, and sample-to-detector 70 cm. To assess the possibility for phase-sensitive, multi-contrast micro-CT on the seconds timescale, a phantom consisting of an LDPE rod, a PVC foam, and a tube of flour was built. The phantom was scanned using 361 projections of 25 ms, distributed across 360°, for a total scan time of 9 s. The source was operated at 50 kV 24 mA.

3. RESULTS

Figure 1 illustrates the results of the fast scans of the static borosilicate sphere phantom. Figure 1a shows axial slices of the reconstructed volumes, where a visual reduction of noise can be seen with increasing acquisition time T_{CT}. The indicated line profiles through the spheres are plotted in 1b, alongside the dashed theoretical profile. The theoretical profile was calculated using the estimated average incident beam energy at the scintillator, using the SpekPy package[37] and tabulated NIST reference data.[38] Discrepancies between the experimental and theoretical profiles can be attributed to the estimated beam energy, which did not accurately model the complicated transfer function of the detector. Assuming sufficient absorption efficiency that all photons in the beam are detected with near unity efficiency, the indirect detection system meant that higher energy photons receive a higher weighting in the integrated signal, shifting the average effective energy upwards. In addition, convolution of the theoretical profile with a PSF (consisting of contributions from detector, source blur, and sample motion) further reduces the peak of the experimental profile by spreading the conserved signal across a large space. This implies that optimisation of the spatial resolution of the system would further enhance the quantitativeness of the results. Figure 1c shows volume renderings of the phantom at each T_{CT}, indicating that morphological features may be identified even with ultra-fast acquisition speeds. Note that it is clear from the full view renderings that increasing detector frame rate required sacrificing vertical FOV due to the necessary sub-array readout.

Reconstructing the volumes using the analytical FDK algorithm ensured that the noise in the volumes reflected the statistics of the measured signal, allowing an analysis of the CNR verus T_{CT}. The results of this analysis are plotted in figure 2, where the error bars indicate the propagated uncertainty (standard deviation) of the measurement repeated on multiple slices. A further data point (in red) is derived from reconstructing using half of the projections from the 132 ms dataset, resulting in an effective 66 ms micro-CT scan. While this particular scan was not physically implemented, the maximum rotation speed of the tomography stage (up to 38 revolutions per second) means that such a scan is readily achievable. The inset illustrates an axial slice from this reconstruction, indicating that when hitting frame-rate induced limits, artefact-free reconstructions of simple samples is still possible by reducing the number of acquired projections. The CNR data points were fitted with a function of the form $a\sqrt{T_{CT}}$, yielding an r^2 value of 0.96. This suggests a noise behaviour predominantly limited by Poisson statistics, as expected in a flux-limited experimental setting like ours.

Figure 3a shows coronal slices at the same sample position at three different time points during the dynamic foam expansion. The volumes were reconstructed using both the analytical FDK algorithm, and SIRT using 40 iterations and a non-negativity constraint. The improvement in CNR of the SIRT reconstruction is very clear, especially with regards to the delineation of the sample from the background (aided by the non-negativity constraint). Additionally, although the spatial resolution was not sufficient to resolve the fine porous structure of the foam, the structure appearing at higher length scales becomes visible. This is made especially clear in the

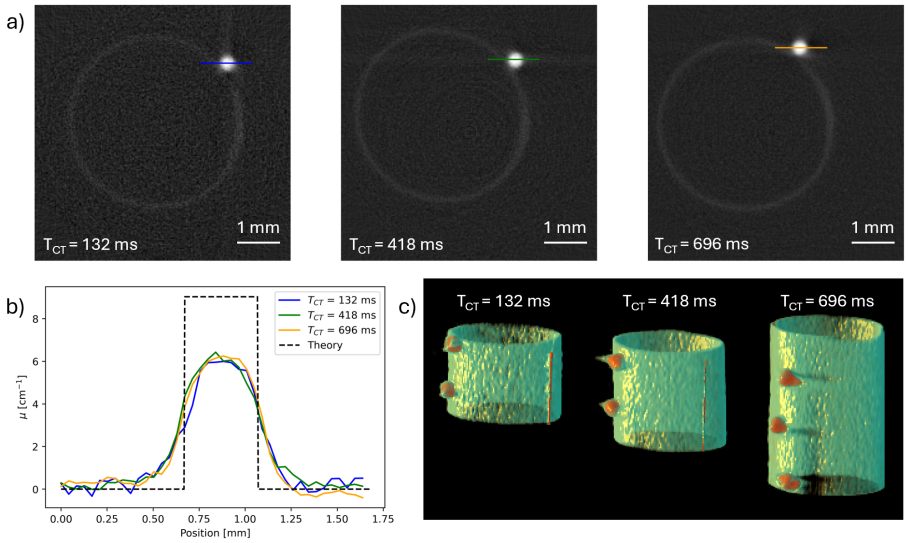

Figure 1: (a) Axial slices of the reconstructions of the statically imaged sphere phantom illustrating the same part of the sample with varying CT acquisition time T_{CT} = 132 ms, 418 ms, 696 ms. (b) Plotted line profiles through the spheres indicated on (a), plotted alongside the theoretical profile of the sphere attenuation for the estimated average incident beam energy. (c) Volume renderings of the sphere phantom derived from the reconstructions.

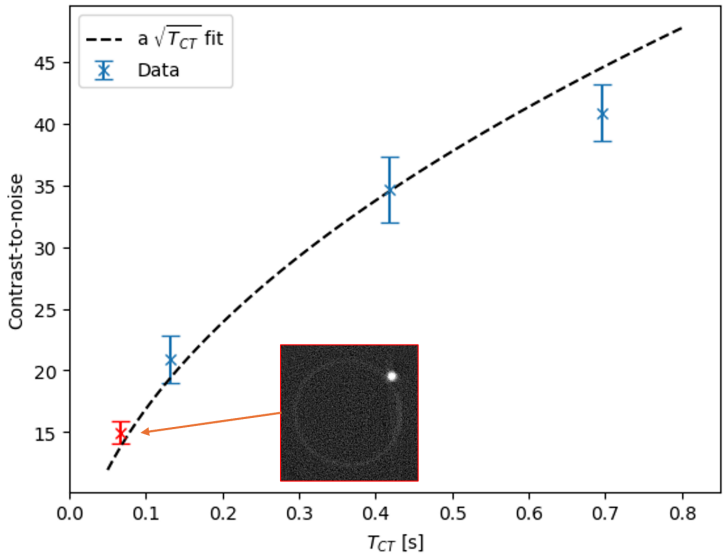

Figure 2: A plot of the contrast-to-noise ratio of the borosilicate sphere versus CT acquisition time. Error bars indicate the propagated uncertainty (standard deviation) of the measurement repeated on multiple slices. The data point indicated in red is derived from a theoretical (yet experimentally implementable) scan obtained from halving the 132 ms dataset, with the inset showing the result of this reconstruction.

supplementary video https://dx.doi.org/10.1117/12.3028059.1, where the sample movement makes the structure most perceptible. The effective delineation from the background made simple grey-value thresholding sufficient to segment the foam. This made possible further analysis, in which the change in attenuation coefficient μ with time could be plotted to understand the expansion dynamics of the sample. Fitting with an equation of the form $\mu = ae^{-T/\tau}$ yielded the time constant describing the decompression process of $\tau = 73.7$ s.

Figure 4 demonstrates the average of three axial slices of the separate attenuation, phase, and dark-field

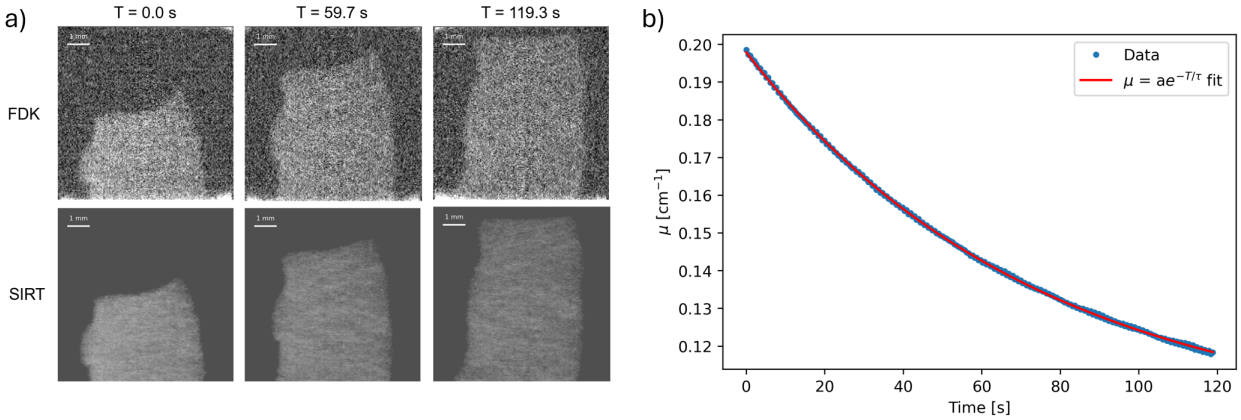

Figure 3: a) Coronal slices of the expanding foam at time points T = 0.0 s, 59.7 s, 119.3 s using both FDK and SIRT algorithms. A video demonstrating the expansion in coronal slices and volume renderings is included in Video 1 https://dx.doi.org/10.1117/12.3028059.1. b) A plot illustrating the temporal evolution of the attenuation coefficient μ, extracted from segmentation of the SIRT reconstructed foam.

reconstructions from the 9 s beam-tracking scan. The phase-contrast channel yielded higher CNR values for the LDPE rod of 6.1 ± 0.5 versus 4.6 ± 0.1 for the same slices in attenuation. Visually, the flour appears slightly better delineated from the surrounding tube in the phase reconstruction, this is despite both contrasts being generated from the same number of photons (and thus dose). While the beam-tracking method also allowed the retrieval of the dark-field channel from the same set of data, the higher noise inherent in this contrast channel meant that a quality reconstruction could not be formed from the limited statistics of the unoptimised 9 s scan. Nevertheless, a faint signal in the position of the flour, a known source of dark-field, is visible in figure 4c.

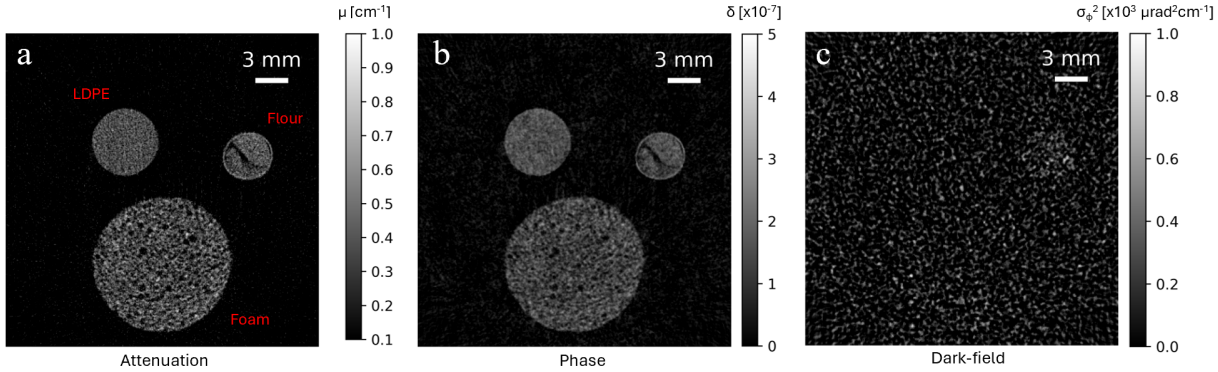

Figure 4: Axial slices of the reconstructed attenuation (a), phase (b), and dark-field (c) volumes from a beam-tracking micro-CT scan acquired in a total time of 9 s. The phantom includes an LDPE rod, a straw filled with flour, and a PVC foam.

4. DISCUSSION

We have demonstrated a custom system for fast micro-CT, achieving a CT acquisition time of 132 ms, which is, to the best of the author's knowledge, the fastest yet demonstrated using a laboratory x-ray source. As a proof of concept of dynamic micro-CT, we applied the system to the task of the 4D measurement of an expanding polymer foam. In the results demonstrated, acquiring sufficient photon statistics for sub-second tomography required compromising on spatial-resolution through the choice of scintillator.

A particularly interesting area for future exploration is the choice of reconstruction algorithm. While analytical reconstruction allowed the reconstruction of the simple sphere phantom from only 66 x 1 ms projections, more complex samples may benefit from specific sparse-view algorithms.[39,40] Furthermore, in dynamic studies the full 4D dataset contains much complementary information across the timesteps. Exploiting this information through 4D reconstruction methods,[41,42] those that consider the temporal as well as spatial dimensions, should result in improved reconstructions compared to the current method which reconstructs independent 3D volumes.

The extension of the system to multi-contrast phase-sensitivity was also demonstrated. Reconstructions of both attenuation and phase were possible from only 9 s of data, many orders of magnitude faster than the typical hours previously demonstrated in beam-tracking experiments.[29,30,43] Despite the success of the attenuation and phase reconstructions, the dark-field channel could not be reconstructed to a good standard due to its inherently lower signal-to-noise ratio. Optimisation of the system geometry, in particular its length,[44] is likely to improve the sensitivity of the system and make dark-field tomography possible over the same timescales. Alternatively, simply relaxing temporal constraints to applications on the minutes timescale[28] could potentially allow the current system to be utilised. Dynamic dark-field tomography could see further application in a range of topics including small animal imaging[25] and materials sciences.[26,27]

The choice to acquire only a single shot per projection angle made fast beam-tracking possible, without the overheads associated with the movement of optical elements. In such a scan, spatial-resolution is limited by the pitch of the mask, yet quantitative information may still be retrieved.[45] Potential future work can explore the implementation of advanced cycloidal acquisition schemes[46] into dynamic beam-tracking imaging, to enhance the spatial resolution achievable with the same number of projections while remaining compatible with flyscan acquisition schemes.

5. CONCLUSION

We have developed a micro-CT system composed of a powerful x-ray source and a custom, flexible detector. A simple phantom was well reconstructed from CT acquisitions as short as 132 ms, with the potential for yet faster scans also demonstrated. This high-speed performance was utilised to carry out 4D imaging of an expanding foam at a 2 Hz CT acquisition rate, allowing an analysis of the change in the volumetric attenuation coefficient over time, and thus helping to develop an understanding of the decompression rate. The system was easily extended to allow multi-contrast phase-sensitive tomography on the seconds timescale. Reconstructions of attenuation, phase, and dark-field volumes suggest that with further optimisation, the system can be utilised for multi-contrast dynamic studies.

ACKNOWLEDGMENTS

This work is supported by the EPSRC-funded UCL Centre for Doctoral Training in Intelligent, Integrated Imaging in Healthcare (i4health) (EP/S021930/1), the Department of Health's NIHR funded Biomedical Research Centre at University College London Hospitals, and the National Research Facility for Lab X-ray CT (NXCT) through EPSRC grants EP/T02593X/1 and EP/V035932/1; and by the Wellcome Trust 221367/Z/20/Z. This work was supported by the Francis Crick Institute which receives its core funding from Cancer Research UK (CC0102), the UK Medical Research Council (CC0102), and the Wellcome Trust (CC0102).

REFERENCES

[1] Withers, P. J., Bouman, C., Carmignato, S., Cnudde, V., Grimaldi, D., Hagen, C. K., Maire, E., Manley, M., Du Plessis, A., and Stock, S. R., "X-ray computed tomography," *Nature Reviews Methods Primers* **1**(1), 18 (2021).

[2] Babin, P., Della Valle, G., Chiron, H., Cloetens, P., Hoszowska, J., Pernot, P., Réguerre, A., Salvo, L., and Dendievel, R., "Fast x-ray tomography analysis of bubble growth and foam setting during breadmaking," *Journal of Cereal Science* **43**(3), 393–397 (2006).

[3] Mokso, R., Marone, F., Haberthür, D., Schittny, J., Mikuljan, G., Isenegger, A., and Stampanoni, M., "Following dynamic processes by x-ray tomographic microscopy with sub-second temporal resolution," in [*AIP conference proceedings*], **1365**(1), 38–41, American Institute of Physics (2011).

[4] Thompson, A., Maskery, I., and Leach, R. K., "X-ray computed tomography for additive manufacturing: a review," *Measurement Science and Technology* **27**(7), 072001 (2016).

[5] Du Plessis, A., Yadroitsev, I., Yadroitsava, I., and Le Roux, S. G., "X-ray microcomputed tomography in additive manufacturing: a review of the current technology and applications," *3D Printing and Additive Manufacturing* **5**(3), 227–247 (2018).

[6] Murrie, R. P., Werdiger, F., Donnelley, M., Lin, Y.-w., Carnibella, R. P., Samarage, C. R., Pinar, I., Preissner, M., Wang, J., Li, J., et al., "Real-time in vivo imaging of regional lung function in a mouse model of cystic fibrosis on a laboratory x-ray source," *Scientific reports* **10**(1), 447 (2020).

[7] Fardin, L., Broche, L., Lovric, G., Mittone, A., Stephanov, O., Larsson, A., Bravin, A., and Bayat, S., "Imaging atelectrauma in ventilator-induced lung injury using 4d x-ray microscopy," *Scientific Reports* **11**(1), 4236 (2021).

[8] Walker, S. M., Schwyn, D. A., Mokso, R., Wicklein, M., Müller, T., Doube, M., Stampanoni, M., Krapp, H. G., and Taylor, G. K., "In vivo time-resolved microtomography reveals the mechanics of the blowfly flight motor," *PLoS biology* **12**(3), e1001823 (2014).

[9] Mokso, R., Schlepütz, C. M., Theidel, G., Billich, H., Schmid, E., Celcer, T., Mikuljan, G., Sala, L., Marone, F., Schlumpf, N., et al., "Gigafrost: the gigabit fast readout system for tomography," *Journal of synchrotron radiation* **24**(6), 1250–1259 (2017).

[10] Yashiro, W., Noda, D., and Kajiwara, K., "Sub-10-ms x-ray tomography using a grating interferometer," *Applied Physics Express* **10**(5), 052501 (2017).

[11] García-Moreno, F., Kamm, P. H., Neu, T. R., Bülk, F., Mokso, R., Schlepütz, C. M., Stampanoni, M., and Banhart, J., "Using x-ray tomoscopy to explore the dynamics of foaming metal," *Nature communications* **10**(1), 3762 (2019).

[12] Endrizzi, M., "X-ray phase-contrast imaging," *Nuclear instruments and methods in physics research section A: Accelerators, spectrometers, detectors and associated equipment* **878**, 88–98 (2018).

[13] Kitchen, M. J., Buckley, G. A., Gureyev, T. E., Wallace, M. J., Andres-Thio, N., Uesugi, K., Yagi, N., and Hooper, S. B., "Ct dose reduction factors in the thousands using x-ray phase contrast," *Scientific reports* **7**(1), 15953 (2017).

[14] Zwanenburg, E., Williams, M., and Warnett, J. M., "Review of high-speed imaging with lab-based x-ray computed tomography," *Measurement Science and Technology* **33**(1), 012003 (2021).

[15] Eggert, A., Müller, M., Nachtrab, F., Dombrowski, J., Rack, A., and Zabler, S., "High-speed in-situ tomography of liquid protein foams," *International journal of materials research* **105**(7), 632–639 (2014).

[16] Dewanckele, J., Boone, M., Coppens, F., Van Loo, D., and Merkle, A., "Innovations in laboratory-based dynamic micro-ct to accelerate in situ research," *Journal of Microscopy* **277**(3), 197–209 (2020).

[17] Bultreys, T., Boone, M. A., Boone, M. N., De Schryver, T., Masschaele, B., Van Hoorebeke, L., and Cnudde, V., "Fast laboratory-based micro-computed tomography for pore-scale research: Illustrative experiments and perspectives on the future," *Advances in water resources* **95**, 341–351 (2016).

[18] Vavřík, D., Jakbek, J., Kumpova, I., and Pichotka, M., "Laboratory based study of dynamical processes by 4d x-ray ct with sub-second temporal resolution," *Journal of Instrumentation* **12**(02), C02010 (2017).

[19] Wilkins, S., Gureyev, T. E., Gao, D., Pogany, A., and Stevenson, A., "Phase-contrast imaging using polychromatic hard x-rays," *Nature* **384**(6607), 335–338 (1996).

[20] Pfeiffer, F., Weitkamp, T., Bunk, O., and David, C., "Phase retrieval and differential phase-contrast imaging with low-brilliance x-ray sources," *Nature physics* **2**(4), 258–261 (2006).

[21] Olivo, A. and Speller, R., "A coded-aperture technique allowing x-ray phase contrast imaging with conventional sources," *Applied Physics Letters* **91**(7), 074106 (2007).

[22] Vittoria, F. A., Kallon, G. K., Basta, D., Diemoz, P. C., Robinson, I. K., Olivo, A., and Endrizzi, M., "Beam tracking approach for single–shot retrieval of absorption, refraction, and dark–field signals with laboratory x–ray sources," *Applied Physics Letters* **106**(22), 224102 (2015).

[23] Pfeiffer, F., Bech, M., Bunk, O., Kraft, P., Eikenberry, E. F., Brönnimann, C., Grünzweig, C., and David, C., "Hard-x-ray dark-field imaging using a grating interferometer," *Nature materials* **7**(2), 134–137 (2008).

[24] Endrizzi, M., Diemoz, P. C., Millard, T. P., Louise Jones, J., Speller, R. D., Robinson, I. K., and Olivo, A., "Hard x-ray dark-field imaging with incoherent sample illumination," *Applied Physics Letters* **104**(2), 024106 (2014).

[25] Velroyen, A., Yaroshenko, A., Hahn, D., Fehringer, A., Tapfer, A., Müller, M., Noël, P., Pauwels, B., Sasov, A., Yildirim, A., et al., "Grating-based x-ray dark-field computed tomography of living mice," *EBioMedicine* **2**(10), 1500–1506 (2015).

[26] Massimi, L., Clark, S. J., Marussi, S., Doherty, A., Schulz, J., Marathe, S., Rau, C., Endrizzi, M., Lee, P. D., and Olivo, A., "Dynamic multicontrast x-ray imaging method applied to additive manufacturing," *Physical Review Letters* **127**(21), 215503 (2021).

[27] Prade, F., Chabior, M., Malm, F., Grosse, C., and Pfeiffer, F., "Observing the setting and hardening of cementitious materials by x-ray dark-field radiography," *Cement and Concrete Research* **74**, 19–25 (2015).

[28] John, D., Gottwald, W., Berthe, D., Wirtensohn, S., Hickler, J., Heck, L., and Herzen, J., "X-ray dark-field computed tomography for monitoring of tissue freezing," *Scientific Reports* **14**(1), 5599 (2024).

[29] Navarrete-León, C., Doherty, A., Savvidis, S., Gerli, M. F., Piredda, G., Astolfo, A., Bate, D., Cipiccia, S., Hagen, C. K., Olivo, A., et al., "X-ray phase-contrast microtomography of soft tissues using a compact laboratory system with two-directional sensitivity," *Optica* **10**(7), 880–887 (2023).

[30] Lioliou, G., Navarrete-León, C., Astolfo, A., Savvidis, S., Bate, D., Endrizzi, M., Hagen, C., and Olivo, A., "A laboratory-based beam tracking x-ray imaging method achieving two-dimensional phase sensitivity and isotropic resolution with unidirectional undersampling," *Scientific Reports* **13**(1), 8707 (2023).

[31] Dreier, E., Bergamaschi, A., Kallon, G. K., Brönnimann, R., Olsen, U. L., Olivo, A., and Endrizzi, M., "Tracking based, high-resolution single-shot multimodal x-ray imaging in the laboratory enabled by the sub-pixel resolution capabilities of the mönch detector," *Applied Physics Letters* **117**(26) (2020).

[32] Morgan, K. S., Paganin, D. M., and Siu, K. K., "X-ray phase imaging with a paper analyzer," *Applied Physics Letters* **100**(12) (2012).

[33] Wen, H., Bennett, E. E., Hegedus, M. M., and Carroll, S. C., "Spatial harmonic imaging of x-ray scattering—initial results," *IEEE transactions on medical imaging* **27**(8), 997–1002 (2008).

[34] Feldkamp, L. A., Davis, L. C., and Kress, J. W., "Practical cone-beam algorithm," *Josa a* **1**(6), 612–619 (1984).

[35] Van Aarle, W., Palenstijn, W. J., Cant, J., Janssens, E., Bleichrodt, F., Dabravolski, A., De Beenhouwer, J., Batenburg, K. J., and Sijbers, J., "Fast and flexible x-ray tomography using the astra toolbox," *Optics express* **24**(22), 25129–25147 (2016).

[36] Vo, N. T., Atwood, R. C., and Drakopoulos, M., "Superior techniques for eliminating ring artifacts in x-ray micro-tomography," *Optics express* **26**(22), 28396–28412 (2018).

[37] Poludniowski, G., Omar, A., Bujila, R., and Andreo, P., "Spekpy v2. 0—a software toolkit for modeling x-ray tube spectra," *Medical Physics* **48**(7), 3630–3637 (2021).

[38] Hubbell, J. and Seltzer, S., "Nist standard reference database 126," *Gaithersburg, MD: National Institute of Standards and Technology* (1996).

[39] Hu, Z., Gao, J., Zhang, N., Yang, Y., Liu, X., Zheng, H., and Liang, D., "An improved statistical iterative algorithm for sparse-view and limited-angle ct image reconstruction," *Scientific reports* **7**(1), 10747 (2017).

[40] Bertram, M., Wiegert, J., Schafer, D., Aach, T., and Rose, G., "Directional view interpolation for compensation of sparse angular sampling in cone-beam ct," *IEEE transactions on medical imaging* **28**(7), 1011–1022 (2009).

[41] Kazantsev, D., Thompson, W. M., Lionheart, W. R., Van Eyndhoven, G., Kaestner, A. P., Dobson, K. J., Withers, P. J., and Lee, P. D., "4d-ct reconstruction with unified spatial-temporal patch-based regularization," *Inverse problems and imaging* **9**(2), 447–467 (2015).

[42] Papoutsellis, E., Ametova, E., Delplancke, C., Fardell, G., Jørgensen, J. S., Pasca, E., Turner, M., Warr, R., Lionheart, W. R., and Withers, P. J., "Core imaging library-part ii: multichannel reconstruction for dynamic and spectral tomography," *Philosophical Transactions of the Royal Society A* **379**(2204), 20200193 (2021).

[43] Vittoria, F. A., Endrizzi, M., Kallon, G. K., Hagen, C. K., Diemoz, P. C., Zamir, A., and Olivo, A., "Beam tracking phase tomography with laboratory sources," *Journal of Instrumentation* **13**(04), C04008 (2018).

[44] Havariyoun, G., Vittoria, F. A., Hagen, C. K., Basta, D., Kallon, G. K., Endrizzi, M., Massimi, L., Munro, P., Hawker, S., Smit, B., et al., "A compact system for intraoperative specimen imaging based on edge illumination x-ray phase contrast," *Physics in Medicine & Biology* **64**(23), 235005 (2019).

[45] Hagen, C., Diemoz, P., Endrizzi, M., and Olivo, A., "The effect of the spatial sampling rate on quantitative phase information extracted from planar and tomographic edge illumination x-ray phase contrast images," *Journal of Physics D: Applied Physics* **47**(45), 455401 (2014).

[46] Hagen, C. K., Vittoria, F. A., Morgó, O. R. i., Endrizzi, M., and Olivo, A., "Cycloidal computed tomography," *Physical Review Applied* **14**(1), 014069 (2020).